Available online at www.sciencedirect.com
ScienceDirect
International Journal of Thermal Sciences 48 (2009) 271–281
International Journal of Thermal Sciences
www.elsevier.com/locate/ijts

# The effect of viscous dissipation and rarefaction on rectangular microchannel convective heat transfer

J. van Rij, T. Ameel *, T. Harman

*Department of Mechanical Engineering, University of Utah, Salt Lake City, UT 84112, USA*

Received 29 March 2008; received in revised form 25 July 2008; accepted 29 July 2008

Available online 21 August 2008

**Abstract**

The effect of viscous dissipation and rarefaction on rectangular microchannel convective heat transfer rates, as given by the Nusselt number, is numerically evaluated subject to constant wall heat flux ($H2$) and constant wall temperature ($T$) thermal boundary conditions. Numerical results are obtained using a continuum based, three-dimensional, compressible, unsteady computational fluid dynamics algorithm with slip velocity and temperature jump boundary conditions applied to the momentum and energy equations, respectively. For the limiting case of parallel plate channels, analytic solutions for the thermally and hydrodynamically fully developed momentum and energy equations are derived, subject to both first- and second-order slip velocity and temperature jump boundary conditions, from which analytic Nusselt number solutions are then obtained. Excellent agreement between the analytical and numerical results verifies the accuracy of the numerical algorithm, which is then employed to obtain three-dimensional rectangular channel and thermally/hydrodynamically developing Nusselt numbers. Nusselt number data are presented as functions of Knudsen number, Brinkman number, Peclet number, momentum and thermal accommodation coefficients, and aspect ratio. Rarefaction and viscous dissipation effects are shown to significantly affect the convective heat transfer rate in the slip flow regime.


*Keywords:* Microchannel; Nusselt number; Slip flow; Brinkman number; Viscous dissipation

## 1. Introduction

Many technological advances in computation speed, power supply requirements, diagnostics, and control issues are contingent on the reduction of thermal fluid systems to the microscale. However, as thermal fluid system sizes are reduced to the microscale, effects that are negligible at a macroscale may become significant, and thus change the predicted behavior of these systems. For gaseous flows, some of these effects include rarefaction, viscous dissipation, compressibility, and axial conduction, which may be characterized by the Knudsen number, $Kn$, Brinkman number, $Br$, Mach number, $Ma$, and Peclet number, $Pe$, respectively. Fundamental to the design of many thermal fluid systems is the accurate evaluation of convective heat transfer rates, typically presented in the form of the Nusselt number, $Nu$. Although, the assessment of gaseous microchannel $Nu$, subject to effects of $Kn$, $Br$, $Ma$, and $Pe$, has been an active area of research, there are currently no experimentally determined values of local convective heat transfer rates, due to measurement and accuracy limitations at the microscale, and rarified microchannel $Nu$ data must generally be acquired analytically or numerically.

The most common means of analytically or numerically modeling a rarified flow within the slip regime, $0.01 \leqslant Kn \leqslant 0.1$, is through the use of slip velocity and temperature jump boundary conditions applied to the conventional continuum momentum and energy equations. The original slip velocity boundary condition, given in Eq. (1), and temperature jump boundary condition, given in Eq. (2), were derived by Maxwell [1] and Smoluchowski [2], respectively.

$$u|_{y=0} - u_w = \left[\left(\frac{2-\sigma_v}{\sigma_v}\right)\frac{\lambda}{\mu}\tau + \frac{3}{4}\frac{\mu R}{P}\frac{\partial T}{\partial x}\right]_{y=0} \tag{1}$$

$$T|_{y=0} - T_w = \left[\left(\frac{2-\sigma_t}{\sigma_t}\right)\left(\frac{2\gamma}{1+\gamma}\right)\frac{\lambda}{Pr}\frac{\partial T}{\partial y}\right]_{y=0} \tag{2}$$

* Corresponding author. Tel.: +1 801 585 9730; fax: +1 801 585 9826.
*E-mail address:* ameel@mech.utah.edu (T. Ameel).

1290-0729/$ – see front matter 
doi:10.1016/j.ijthermalsci.2008.07.010

**Nomenclature**

| | | |
|---|---|---|
| $AR$ | aspect ratio, $b/h$ | |
| $b$ | channel width | m |
| $Br$ | Brinkman number, $Br_{H2} = \mu u_m^2/(q_w D_h)$, $Br_T = \mu u_m^2/(k(T_i - T_w))$ | |
| $c_p$ | specific heat at constant pressure | $\mathrm{J\,kg^{-1}\,K^{-1}}$ |
| $c_v$ | specific heat at constant volume | $\mathrm{J\,kg^{-1}\,K^{-1}}$ |
| $D_h$ | hydraulic diameter, $2bh/(b+h)$ | m |
| $e$ | internal energy per unit mass | $\mathrm{J\,kg^{-1}}$ |
| $h$ | channel height | m |
| $k$ | thermal conductivity | $\mathrm{W\,m^{-1}\,K^{-1}}$ |
| $Kn$ | Knudsen number, $\lambda/D_h$ | |
| $L$ | channel length | m |
| $Ma$ | Mach number, $(Kn\,Pe/Pr)\sqrt{2/(\pi\gamma)}$ | |
| $Nu$ | Nusselt number, $q_{w,m} D_h/(k(T_w - T_m))$ | |
| $P$ | pressure | Pa |
| $Pe$ | Peclet number, $Pr\,Re$ | |
| $Pr$ | Prandtl number, $c_p\mu/k$ | |
| $q$ | heat flux | $\mathrm{W\,m^{-2}}$ |
| $R$ | gas constant | $\mathrm{J\,kg^{-1}\,K^{-1}}$ |
| $Re$ | Reynolds number, $\rho u_m D_h/\mu$ | |
| $T$ | temperature | K |
| $t$ | time | s |
| $u$ | velocity in $x$-direction | $\mathrm{m\,s^{-1}}$ |
| $v$ | velocity in $y$-direction | $\mathrm{m\,s^{-1}}$ |
| $\mathbf{v}$ | velocity vector | $\mathrm{m\,s^{-1}}$ |
| $x, y, z$ | Cartesian coordinates | m |

*Greek symbols*

| | | |
|---|---|---|
| $\beta$ | gas–wall interaction parameter, $\beta_{t1}/\beta_{v1}$ | |
| $\beta_{t1}$ | first-order temperature jump coefficient, $((2-\sigma_t)/\sigma_t)(2\gamma/(1+\gamma))(1/Pr)$ | |
| $\beta_{t2}$ | second-order temperature jump coefficient | |
| $\beta_{v1}$ | first-order velocity slip coefficient, $(2-\sigma_v)/\sigma_v$ | |
| $\beta_{v1}Kn$ | rarefaction parameter | |
| $\beta_{v2}$ | second-order velocity slip coefficient | |
| $\gamma$ | ratio of specific heats, $c_p/c_v$ | |
| $\lambda$ | molecular mean free path, $\mu/(\rho\sqrt{2RT/\pi})$ | m |
| $\mu$ | dynamic viscosity | $\mathrm{kg\,m^{-1}\,s^{-1}}$ |
| $\rho$ | density | $\mathrm{kg\,m^{-3}}$ |
| $\sigma_t$ | thermal accommodation coefficient | |
| $\sigma_v$ | momentum accommodation coefficient | |
| $\boldsymbol{\tau}$ | shear stress | Pa |
| $\Phi$ | viscous dissipation term, $\nabla\cdot(v\cdot\tau) - v\cdot(\nabla\cdot\tau)$ | $\mathrm{J\,m^{-3}\,s^{-1}}$ |

*Subscripts*

| | |
|---|---|
| $H2$ | constant wall heat flux condition |
| $i$ | inlet value |
| $m$ | mean value |
| $o$ | outlet value |
| $T$ | constant wall temperature condition |
| $w$ | wall value |
| $\infty$ | fully developed value |

*Superscripts*

| | |
|---|---|
| 0 | initial value |

The first term in Eq. (1) is the velocity slip due to the shear stress at the wall, and the second term is the thermal creep velocity due to a temperature gradient tangential to the wall. Eqs. (1) and (2), as well as subsequent equations, are presented in a format assuming a Cartesian coordinate system, a wall normal direction ($y$), and a streamwise direction ($x$) (see Fig. 1). To reduce the number of variables involved, the nondimensional parameters $\beta_{v1}$, $\beta_{t1}$, $\beta_{v1}Kn$, and $\beta$, as defined in the nomenclature, are used hereafter, rather than the coefficients of Eqs. (1) and (2). $\beta_{v1}Kn$ is representative of the level of rarefaction, where $\beta_{v1}Kn = 0$, corresponds to continuum conditions, and $\beta_{v1}Kn \approx 0.10$, corresponds to the approximate upper limit of the slip regime. $\beta$ is representative of the gas–wall interactions, where $\beta = 0$ corresponds to the artificial condition of zero temperature jump with nonzero slip velocity, $\beta \approx 1.667$ corresponds to typical values for air ($\gamma = 1.4$, $Pr = 0.7$) when $\sigma_v = \sigma_t = 1$, and $\beta$ values as high as 100 are possible (depending on the relative magnitudes of $\gamma$, $Pr$, $\sigma_v$ and $\sigma_t$, where values of $\sigma_v$ and $\sigma_t$ must be measured experimentally, and are presented for several common fluid-surface interactions in [3]).

In addition to the first-order slip model given by Eqs. (1) and (2), numerous second-order models and modifications have been proposed to improve the accuracy and range of applicability of the slip flow representation of rarefaction into the lower transition regime [3]. These second-order boundary condition models are often compared for two-dimensional, planar, constant property flow, without creep flow. For this configuration, many second-order models may be written in the format of Eqs. (3) and (4), where values of $\beta_{v2}$ and $\beta_{t2}$ depend on the second-order model.

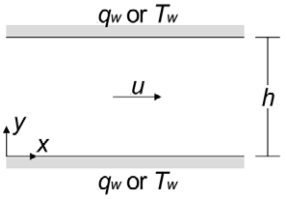


Fig. 1. Two-dimensional channel configuration.

$$u|_{y=0} - u_w = \left[\beta_{v1}\lambda\frac{\partial u}{\partial y} - \beta_{v2}\lambda^2\frac{\partial^2 u}{\partial y^2}\right]_{y=0} \tag{3}$$

$$T|_{y=0} - T_w = \left[\beta_{t1}\lambda\frac{\partial T}{\partial y} - \beta_{t2}\lambda^2\frac{\partial^2 T}{\partial y^2}\right]_{y=0} \tag{4}$$

Currently, there is insufficient experimental data to establish the use of any particular second-order model over another.

Nonetheless, several evaluations have shown second-order boundary conditions to be useful with respect to evaluating microchannel mass flow rates [4,5], and as such, theoretical convective heat transfer solutions with second-order terms may prove valuable as additional experimental and theoretical results become available.

Viscous dissipation effects in macroscale systems are typically only significant for high velocity or highly viscous flows. In microscale systems, however, large channel length to hydraulic diameter ratios result in large velocity and pressure gradients, and consequently thermal energy generation due to viscous dissipation. A slight increase in fluid temperature may be significant relative to the small temperature gradients typically present in microchannels, and as a result alter the convective heat transfer rate and any temperature dependent fluid properties. Because the function of many microfluidic systems is cooling, viscous dissipation becomes a limiting factor that must be accurately represented. Recently, several theoretical studies have focused specifically on the effects of viscous dissipation in the slip flow regime [6–11]. All of these studies are for parallel plate flow, except for [7], which examines the effect of viscous dissipation for rectangular microchannels and the $H1$ thermal boundary condition. Also, nearly all of these previous studies evaluated the effect of viscous dissipation without also considering the related flow work and shear work effects, which for a rarified gas flow are of the same order of magnitude as viscous dissipation [6,12,13].

The significance of both compressibility and streamwise conduction effects may be established by the magnitude of $Pe$, which is directly related to $Ma$ for a given $Kn$, $Ma = (Kn\,Pe/Pr)\sqrt{2/(\pi\gamma)}$. $Pe$ represents the ratio of thermal energy convected to the fluid to thermal energy axially conducted within the fluid. A low $Pe$, corresponding to a low $Ma$, which is common in micro flows, and generally indicates that compressibility effects are less significant while streamwise conduction effects are nonnegligible. Prior studies indicate that axial conduction effects at low $Pe$ result in an increase in $Nu$ for constant wall temperature thermal boundary conditions [13,14]. Numerical studies which have examined the effects of compressibility in microchannels found that, although compressible flow never reaches a fully developed state, compressible flow at low Mach numbers, 'nearly incompressible flow,' may reach a 'locally fully developed' state, for which the local values of wall friction and heat transfer are approximately equivalent to incompressible values [15,16].

The objective of this study is to numerically evaluate the effects of rarefaction and viscous dissipation for nearly incompressible, rectangular microchannel convective heat transfer rates in the slip flow regime, subject to constant wall heat flux ($H2$) and constant wall temperature ($T$) thermal boundary conditions [13]. Numerical results are obtained using a three-dimensional, compressible, unsteady computational fluid dynamics algorithm. Continuum based conservation equations, constitutive models (Newtonian–Fourier), and equation-of-state model (ideal gas), with slip velocity and temperature jump boundary conditions are utilized, based on the assumption that these approximations are reasonably accurate within the slip flow regime. To verify the numerical results, analytic solutions for thermally and hydrodynamically fully developed parallel plate constant wall heat flux and constant wall temperature Nusselt numbers are derived as a function of rarefaction ($\beta_{v1}Kn$), viscous dissipation ($Br$), gas–wall interactions ($\beta$), and second-order velocity slip and temperature jump terms ($\beta_{v1}$, $\beta_{t2}$). Second-order terms are retained in this analytic analysis to provide a possible basis of comparison for future experimental results, beyond this however, the effect of second-order terms is not investigated in this study. Following the algorithm verification, three-dimensional rectangular microchannel and thermally/hydrodynamically developing Nusselt number data are numerically evaluated and presented as functions of $\beta_{v1}Kn$, $\beta$, $Br$, $Pe$, and aspect ratio, $AR$. Viscous dissipation effects are examined in conjunction with flow work effects, which previous studies have neglected. Compressibility, axial conduction, and creep flow effects are not directly considered in this study, however, due to the low $Ma$ (low $Pe$) utilized to achieve nearly incompressible flow, axial conduction effects will be evident in the constant wall temperature $Nu$ results.

## 2. Analytic solutions

The flow configuration that is analytically evaluated is a two-dimensional parallel-plate microchannel of separation distance $h$, as illustrated in Fig. 1. To obtain analytic solutions, the following simplifying assumptions are applied: two-dimensional, steady state, incompressible, thermally and hydrodynamically fully developed, Newtonian, ideal gas, constant properties, laminar flow, and either symmetrically constant wall heat flux or constant wall temperature. With these simplifications the momentum equation is given in Eq. (5) and the energy equation, in terms of temperature, with viscous dissipation, $\mu(\partial u/\partial y)^2$, and flow work, $u\partial P/\partial x$, terms is given in Eq. (6).

$$\mu\frac{\partial^2 u}{\partial y^2} = \frac{dP}{dx} \tag{5}$$

$$k\frac{\partial^2 T}{\partial y^2} = u\rho c_p\frac{\partial T}{\partial x} - u\frac{\partial P}{\partial x} - \mu\left(\frac{\partial u}{\partial y}\right)^2 \tag{6}$$

With symmetry applied at the microchannel midplane, and the general second-order slip velocity boundary condition, Eq. (3), applied at the wall, the momentum equation, Eq. (5), may be integrated twice to obtain the nondimensional velocity profile given in Eq. (7), in terms of the slip velocity to mean velocity ratio, $u_s/u_m$, Eq. (8).

$$\frac{u(y/h)}{u_m} = \frac{u_s}{u_m} + 6\left(1 - \frac{u_s}{u_m}\right)\left(\frac{y}{h} - \frac{y^2}{h^2}\right) \tag{7}$$

$$\frac{u_s}{u_m} = 1 - \frac{1}{1 + 12\beta_{v1}Kn + 48\beta_{v2}Kn^2} \tag{8}$$

The velocity profile, Eq. (7), is then substituted into the energy equation, Eq. (6). For the fully developed constant wall heat flux case both the pressure and temperature gradients in the $x$-direction are constants, and for the fully developed constant wall temperature case the pressure gradient in the $x$-direction

is constant, and the temperature gradient in the $x$-direction approaches zero. In either case, the energy equation, Eq. (6), may be integrated twice by applying the general second-order temperature jump boundary condition, Eq. (4), at the wall and symmetry at the midplane. The resulting nondimensional temperature profile for constant wall heat flux is given in Eq. (9), with the ensuing $Nu_{H2}$ given in Eq. (10), and the constant wall temperature nondimensional temperature profile is given in Eq. (11), with the subsequent $Nu_T$ given in Eq. (12).

$$\begin{aligned}\frac{T(y/h)-T_w}{q_w D_h/k} = &-\frac{1}{2}\left(\frac{y}{h}-\frac{y^2}{h^2}\right)\\ &\times\left\{1+\left[1+12Br_{H2}\left(3-\frac{u_s}{u_m}\right)\left(1-\frac{u_s}{u_m}\right)\right]\right.\\ &\left.\times\left(1-\frac{u_s}{u_m}\right)\left(\frac{y}{h}-\frac{y^2}{h^2}\right)\right\}\\ &-\beta_{t1}Kn-4\beta_{t2}Kn^2\left[\frac{u_s}{u_m}\right.\\ &\left.-12Br_{H2}\left(3-\frac{u_s}{u_m}\right)\left(1-\frac{u_s}{u_m}\right)^2\right]\end{aligned} \tag{9}$$

$$\begin{aligned}Nu_{H2} = 420\Bigg[&51+420\beta_{t1}Kn-2\frac{u_s}{u_m}\left(9-\frac{u_s}{u_m}-840\beta_{t2}Kn^2\right)\\ &+12Br_{H2}\left(3-\frac{u_s}{u_m}\right)\left(1-\frac{u_s}{u_m}\right)^2\\ &\times\left(9-2\frac{u_s}{u_m}-1680\beta_{t2}Kn^2\right)\Bigg]^{-1}\end{aligned} \tag{10}$$

$$\begin{aligned}\frac{T(y/h)-T_w}{T_i-T_w} = &-6Br_T\left(1-\frac{u_s}{u_m}\right)\left[3\left(1-\frac{y}{h}\right)^2\frac{y^2}{h^2}\right.\\ &-24\beta_{t2}Kn^2\\ &+\frac{u_s}{u_m}\left\{\left(\frac{y}{h}-\frac{y^2}{h^2}\right)\left[1-3\left(\frac{y}{h}-\frac{y^2}{h^2}\right)\right]\right.\\ &\left.\left.+2\beta_{t1}Kn+32\beta_{t2}Kn^2\right\}\right]\end{aligned} \tag{11}$$

$$\begin{aligned}Nu_T = 420\frac{u_s}{u_m}\Bigg[&27-5040\beta_{t2}Kn^2\\ &+\left(9+420\beta_{t1}Kn+6720\beta_{t2}Kn^2\right)\frac{u_s}{u_m}-\frac{u_s^2}{u_m^2}\Bigg]^{-1}\end{aligned} \tag{12}$$

$Nu_{H2}$, Eq. (10) and $Nu_T$, Eq. (12), with $u_s/u_m$ defined in Eq. (8), represent the energy exchange of constant wall heat flux and constant wall temperature, thermally and hydrodynamically fully developed parallel plate microchannel flows. These interactions are a result of the combined effects of rarefaction ($Kn$), the slip flow model parameters ($\beta_{v1}$, $\beta_{v2}$, $\beta_{t1}$, and $\beta_{t2}$), and viscous dissipation, flow work, and shear work ($Br$). Viscous dissipation acts as a distributed heat source, with the majority of the thermal energy generated near the wall, due to the larger velocity gradients. Flow work acts as a distributed heat sink, with the majority of the thermal energy absorbed near the center of the flow, due to the larger velocity magnitudes. And, shear work, $u\partial\tau/\partial y|_{y=0}$, acts as a heat source at the wall, due to the thermal energy generated by the slipping flow. For fully developed, continuum flow there is no shear work at the wall, and the thermal energy generated by viscous dissipation is exactly equal to the thermal energy absorbed by flow work, regardless of the magnitude of $Br$, as discussed in [12] and [13]. Within the slip flow regime, the thermal energy generated by viscous dissipation and shear work is exactly equal to the thermal energy absorbed by flow work, again regardless of the magnitude of $Br$, as discussed in [6].

For continuum flow ($Kn = 0$), with negligible viscous dissipation ($Br_{H2} = 0$), $Nu_{H2}$, Eq. (10), reduces to the conventional value of 8.235. For continuum flow with viscous dissipation, $Nu_{H2}$ reduces to the equation given by [13] for two-dimensional flow with viscous dissipation. For slip flow with first-order terms only ($\beta_{v2} = \beta_{t2} = 0$) and no viscous dissipation, $Nu_{H2}$ reduces to the equation originally derived by Inman [17] (with $Kn = \lambda/h$, rather than $Kn = \lambda/D_h$ used here). When both viscous dissipation and flow work are considered in the continuum flow regime, the energy added by viscous dissipation is equal to the energy absorbed by flow work and, as a result, the fully developed mean temperature is not a function of $Br_{H2}$. The temperature distribution and wall temperature, however, do vary with $Br_{H2}$, and as such, $Nu_{H2}$ is a function of $Br_{H2}$. If the flow work contribution to the energy exchange, $u\partial P/\partial x$, is neglected in the previous analysis, both the wall temperature and the mean temperature are shifted by equal amounts [12] (from their values when both viscous dissipation and flow work are considered), and as a result the nondimensional temperature distribution and $Nu_{H2}$ remain the same as given in Eqs. (9) and (10).

For continuum flow, $Nu_T$, Eq. (12), reduces to zero, which is consistent with results presented in [12] and [13]. $Nu_T = 0$ is notably different from 7.54, the typical $Nu_T$ value reported for constant wall temperature parallel plate flow without axial conduction effects. This is, again, a result of the competing effects of viscous dissipation and flow work, which result in $\partial T_m/\partial x = 0$, $\partial T/\partial y|_{y=0} = 0$, and consequently $Nu_T = 0$, regardless of the magnitude of $Br_T$ or $Pe$. The temperature profile, however, is not uniform, and for $Br_T \neq 0$ the fully developed mean temperature, $T_m$, is always less than the wall temperature, $T_w$, by an amount dependent on the magnitude of $Br_T$. If the flow work term, $u\partial P/\partial x$, is neglected in the preceding derivation, $T_m$ is always greater than $T_w$ by an amount dependent on the magnitude of $Br_T$, and the resulting $Nu_T$ is given by Eq. (13).

$$Nu_T = 140\left(8+140\beta_{t1}Kn+1680\beta_{t2}Kn^2-\frac{u_s}{u_m}\right)^{-1} \tag{13}$$

For continuum flow, Eq. (13) reduces to 17.5, which is consistent with results presented in [8,9,11]. However, rarified flows are generally gaseous, and flow work in gaseous flows is of the same order of magnitude as viscous dissipation. For this reason, it is expected that Eq. (12) is a more accurate representation of the energy exchange in the slip flow regime than Eq. (13).

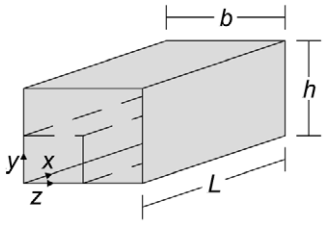


Fig. 2. Rectangular channel configuration.

## 3. Numerical model

The computational fluid dynamics (CFD) algorithm used for this study has been described and verified for previous microchannel investigations [18–21]. The algorithm is a finite volume, multi-material CFD code based on the ICE (Implicit, Continuous-fluid, Eulerian) method. The ICE implementation used in this study is well developed and documented [22–24]. The code is three-dimensional, fully compressible, unsteady, and capable of modeling variable fluid properties, fluid-structure interactions, and chemical reactions. To accurately model microchannel flows, the algorithm has been modified to selectively model first- or second-order slip boundary conditions, creep flow, and viscous dissipation. The implementation of these modifications is consistent with the original code in being numerically second-order accurate both spatially and temporally.

### 3.1. Model parameters and criteria

The flow configuration that is numerically analyzed is illustrated in Fig. 2, and is modeled assuming laminar flow of a Newtonian, ideal gas, with constant properties of air ($\gamma = 1.4$, $Pr = 0.7$), and a uniformly spaced computational grid. For this flow, the governing mass, momentum, and energy equations that are numerically solved are given in Eqs. (14), (15), and (16) respectively.

$$\frac{\partial \rho}{\partial t} + \nabla \cdot (\rho \mathbf{v}) = 0 \tag{14}$$

$$\frac{\partial (\rho \mathbf{v})}{\partial t} + \nabla \cdot (\rho\, \mathbf{v}\mathbf{v}) = -\nabla P + \nabla \cdot \boldsymbol{\tau} \tag{15}$$

$$\frac{\partial (\rho e)}{\partial t} + \nabla \cdot (\rho \mathbf{v} e) = -P(\nabla \cdot \mathbf{v}) + \nabla \cdot (k \nabla T) + \Phi \tag{16}$$

To decrease the computational time required to reach a solution, only one quarter of the symmetric microchannel is modeled. (For parallel plate flows, the model is two-dimensional, and one half of the microchannel is modeled.) Two types of problems are numerically evaluated, thermally developing flows and thermally/hydrodynamically developing flows. For both cases the outlet pressure, along with either the inlet pressure or the inlet velocity, are specified to obtain a given flow *Pe*, *Br* and *Kn*. At the channel wall, either a uniform heat flux or a constant wall temperature is specified. For thermally developing flows a inlet pressure and a uniform inlet temperature are specified while the outlet temperature and the inlet and outlet velocities are allowed to evolve to their fully developed profiles. For combined thermally/hydrodynamically developing flows both a uniform inlet temperature and a uniform inlet velocity are specified while the outlet temperature and velocity are allowed to evolve to their fully developed profiles. An example of the required numerical parameters, and the resulting nondimensional parameters, is given in Table 1 for one set of conditions – a thermally/hydrodynamically developing, constant wall temperature flow.

For the numerical results to be comparable to the analytic solutions, the flow must be locally fully developed, steady state, nearly incompressible, and have constant properties. Given these stipulations, the flow *Pe* and wall heat flux, or wall temperature, are specified such that the total density change within the flow is less than a few percent, and the *Ma* is generally less than approximately 0.05. For the low *Pe* values used in this study, channel lengths of $4h$ for parallel plate channels, and $6h$ for rectangular channels, were found to be sufficient for the flow to develop while avoiding significant compressibility effects due to a longer channel. Because the algorithm is unsteady, flow properties must evolve from a set of initial conditions to steady state conditions subject to the boundary conditions. For all of the data presented, the initial velocity field is zero and the

Table 1
Example computational and nondimensional problem specification for a thermally/hydrodynamically developing, constant wall temperature flow

| Computational problem specification | | |
|---|---|---|
| Inlet boundary | Outlet boundary | Wall boundary |
| $\partial P/\partial x\|_{x=0} = 0.0$ (Pa m$^{-1}$) | $P_o = 82745.4329$ (Pa) | $\partial P/\partial y\|_{y=0} = 0.0$ (Pa m$^{-1}$) |
| $\partial \rho/\partial x\|_{x=0} = 0.0$ (kg m$^{-4}$) | $\partial \rho/\partial x\|_{x=L} = 0.0$ (kg m$^{-4}$) | $\partial \rho/\partial y\|_{y=0} = 0.0$ (kg m$^{-4}$) |
| $T_i = 300.155907$ (K) | $\partial T/\partial x\|_{x=L} = 0.0$ (K m$^{-1}$) | $T\|_{y=0} = T_w + \beta_{t1}\lambda \partial T/\partial y\|_{y=0}$ (K)<br>$T_w = 300$ (K), $\sigma_t = 1.0$ |
| $u_i = 6.68919094$ (m s$^{-1}$) | $\partial u/\partial x\|_{x=L} = 0.0$ (m s$^{-1}$) | $u\|_{y=0} = u_w + \beta_{v1}(\lambda/\mu)\tau\|_{y=0}$ (m s$^{-1}$)<br>$u_w = 0.0$ (m s$^{-1}$), $\sigma_v = 1.0$ |
| Initial conditions | Grid parameters | Fluid properties |
| $\rho^0 = 0.96103871$ (kg m$^{-3}$) | $b = \infty$ (m) (*symmetry*) | $c_v = 717.5$ (J kg$^{-1}$ K$^{-1}$) |
| $T^0 = 300.155907$ (K) | $h/2 = 0.5 \cdot 10^{-6}$ (m) | $k = 0.02583$ (W m$^{-1}$ K$^{-1}$) |
| $u^0 = 0.0$ (m s$^{-1}$) | $L = 4.0 \cdot 10^{-6}$ (m) | $\gamma = 1.4$ |
| | $\Delta x = \Delta y = (h/2)/40$ (m) | $\mu = 1.8 \cdot 10^{-5}$ (kg m$^{-1}$ s$^{-1}$) |
| Nondimensional problem specification | | |
| $AR = \infty$, $\beta_{v1} Kn = 0.04$, $\beta = 1.667$, $Pe = 0.5$, $Br_T = 0.2$ | | |

initial temperature field is equal to the inlet temperature. The magnitude and number of time steps required to reach steady state are dependent on the grid resolution, $Kn$, and $Pe$. The convergence criteria for each time step is a mass flux residual less than $10^{-9}$ for each control volume. The criterion used to establish that the flow is steady state is $|(u^{n+1} - u^n)/u^{n+1}| \leqslant 10^{-10}$ and $|(T^{n+1} - T^n)/T^{n+1}| \leqslant 10^{-10}$, for each control volume, where $n$ is the number of the time step.

### 3.2. Model verification and grid resolution

The algorithm's ability to model the effects of the first- and second-order slip boundary conditions and creep flow, for two-dimensional constant wall heat flux flows was demonstrated in [18]. To establish that the algorithm also accurately models the effects of viscous dissipation, numerically and analytically computed nondimensional temperature profiles are compared in Fig. 3, for several representative cases. The numerically computed values, presented as symbols, are the result of thermally developing parallel plate flow at $x = 3.75h$ and $Pe = 0.5$. The analytically computed values, Eq. (9) in Fig. 3(a), and Eq. (11) in Fig. 3(b), are presented as lines. Based on this comparison, the differences between the analytically and numerically computed temperature profiles are negligible, thereby verifying the ability of the algorithm to model viscous dissipation effects.

To verify that the algorithm is capable of modeling convective heat transfer in rectangular microchannels, and to determine the grid resolution required to do so, grid resolution studies for fully developed, continuum flow $Nu_{H2}$ and $Nu_T$ are presented in Table 2. These data are obtained for $Pe = 0.5$, without viscous dissipation effects. The numerical $Nu_{H2}$ are compared to the analytically determined values given by [13]. At $Pe = 0.5$ axial conduction effects in $Nu_T$ are nonnegligible and analytic solutions are unavailable; $Nu_T$ data are instead compared to the correlation values given by [14], which are reported to include axial conduction effects and to be within 8% of accurate. The data in Table 2 indicate that the numerical algorithm converges with approximately second-order numerical accuracy, and that at the highest grid resolution $Nu_{H2}$ are within 0.1% of analytic solutions, and $Nu_T$ are within 2.2% of correlation values. This indicates that the finest grid resolution for each $AR$ is sufficiently accurate and, consequently, all of the following numerical results are obtain at this resolution (equivalently, for $AR = \infty$ the grid is $320 \times 40 \times 1$).

## 4. Results and discussion

### 4.1. Locally fully developed Nu

Locally fully developed values of $Nu_{H2}$ and $Nu_T$ are presented in Fig. 4 for the specified $AR$, $\beta_{v1}Kn, \beta, Br$, and $Pe$ values. $Nu_{H2}$ and $Nu_T$ for $AR = \infty$, 5, 2, and 1 are given in Figs. 4(a), 4(b), 4(c), and 4(d), respectively, and although each data set exhibits similar trends in $\beta_{v1}Kn$, $\beta$, and $Br$, the effect of $AR$ is significant, and the scaling of each plot should be noted. For these data, first-order slip boundary conditions, without creep flow, are used. Numerically computed values are given by

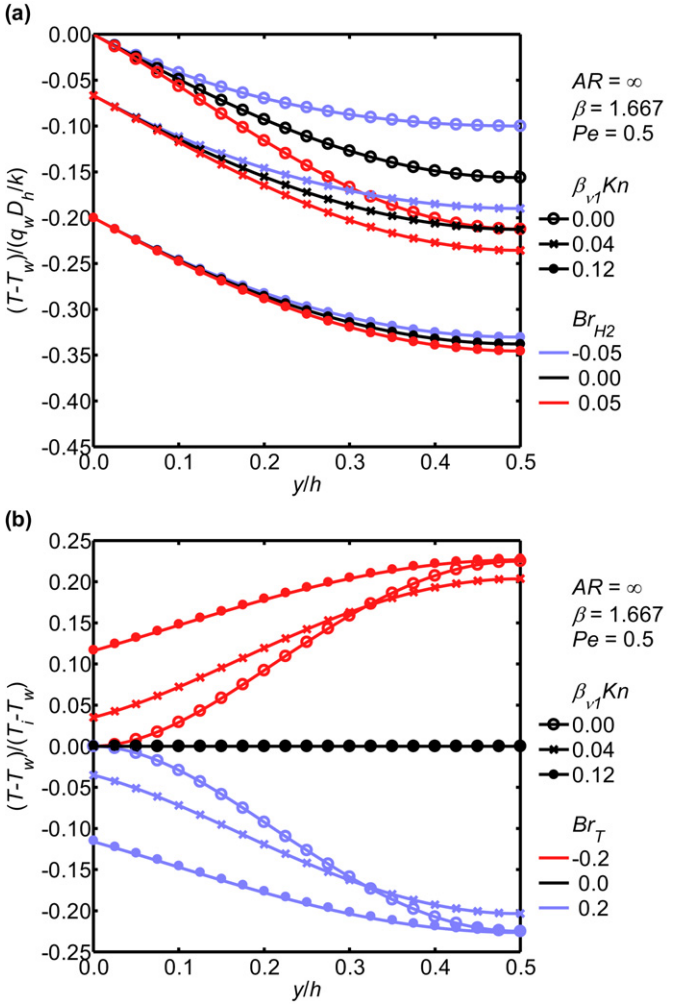


Fig. 3. Comparison of analytical and numerical temperature profiles: (a) constant wall heat flux, Eq. (9), (b) constant wall temperature, Eq. (11).

Table 2
Grid resolution and numerical accuracy study, $Kn = 0$, $Pe = 0.5$, $Br = 0$

| | Grid | $Nu_{H2}$, present | $Nu_{H2}$, [13] | $Nu_T$, present | $Nu_T$, [14] |
|---|---|---|---|---|---|
| $AR = 1$ | $120 \times 10 \times 10$ | 3.175 | 3.09 | 3.404 | 3.293 |
| | $240 \times 20 \times 20$ | 3.108 | | 3.372 | |
| | $480 \times 40 \times 40$ | 3.092 | | 3.364 | |
| $AR = 2$ | $120 \times 10 \times 20$ | 3.070 | 3.02 | 3.853 | 3.849 |
| | $240 \times 20 \times 40$ | 3.031 | | 3.835 | |
| | $480 \times 40 \times 80$ | 3.022 | | 3.831 | |
| $AR = 5$ | $120 \times 10 \times 50$ | 2.964 | 2.93 | 5.455 | 5.405 |
| | $240 \times 20 \times 100$ | 2.936 | | 5.447 | |
| | $480 \times 40 \times 200$ | 2.929 | | 5.445 | |

symbols, with the connecting lines representing the data trend; except in the case of parallel plate flow, $AR = \infty$, for which the lines are the previous derived analytic $Nu$ solutions, Eqs. (10), (12), and (13). For $AR = \infty$, Fig. 4(a), the average difference between the analytic and numeric $Nu_{H2}$ is 0.35%, and the maximum is 1.43%. The average difference between the analytic and numeric $Nu_T$ is 0.28%, and the maximum in 1.03%. Also, in Fig. 4(a), $Nu_T$ derived with viscous dissipation effects, but

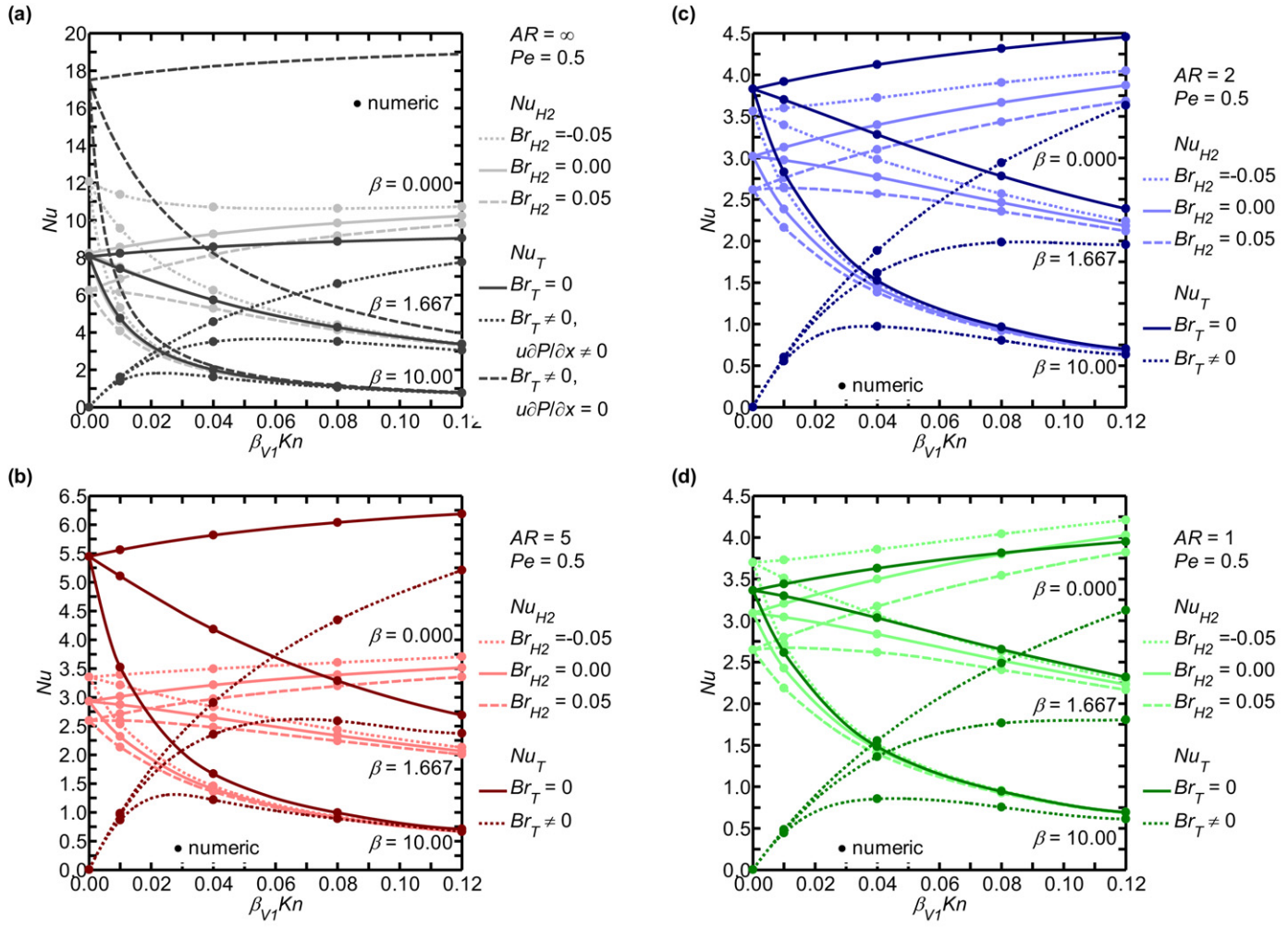


Fig. 4. Effect of viscous dissipation and rarefaction on fully developed $Nu_{H2}$ and $Nu_T$: (a) $AR = \infty$, (b) $AR = 5$, (c) $AR = 2$, (d) $AR = 1$.

without flow work effects, Eq. (13), serves as a comparison to $Nu_T$ given by Eq. (12), which includes both viscous dissipation and flow work effects and is assumed to be the more accurate representation of the thermal energy exchange in constant wall temperature rarified flows.

The $Nu_{H2}$ and $Nu_T$ data in Fig. 4 without viscous dissipation effects, $Br = 0$, demonstrate that as rarefaction, $\beta_{v1}Kn$, increases, $Nu$ may increase or decrease, depending on $\beta$. Increasing rarefaction increases the slip velocity, which increases the energy exchange near the wall and tends to increase $Nu$, as displayed when $\beta = 0$, for all $AR$. However, for $\beta \neq 0$, an increase in rarefaction also increases the temperature jump at the wall. An increase in the temperature jump reduces the energy exchange, increases the mean temperature difference $|T_w - T_m|$, and tends to decrease $Nu$, particularly for large $\beta$. These trends are consistent with previously reported slip flow $Nu$ data, without viscous dissipation effects [25].

The $Nu_{H2}$ data in Fig. 4 with viscous dissipation effects, $Br \neq 0$, indicate that for all $AR$ and $\beta_{v1}Kn$ values investigated, positive $Br_{H2}$, heating, decreases $Nu_{H2}$, and negative $Br_{H2}$, cooling, increases $Nu_{H2}$. As discussed previously, viscous dissipation generates thermal energy predominantly near the wall. This results in an increase in the fluid temperature at the wall, which for heating, increases the difference between the mixed mean fluid temperature and the average wall temperature, thereby reducing $Nu_{H2}$; while for cooling, this decreases the difference between the mixed mean fluid temperature and the average wall temperature, thereby increasing $Nu_{H2}$ (see Fig. 3(a)). The data in Fig. 4 also indicate that viscous dissipation effects are reduced for increasing $\beta_{v1}Kn$. For $AR = \infty$ and $\beta_{v1}Kn = 0.00$, a $Br_{H2}$ of $\pm 0.05$ will produce a 24.1% decrease in $Nu_{H2}$ for heating, and a 46.6% increase in $Nu_{H2}$ for cooling, while at $\beta_{v1}Kn = 0.12$ ($\beta = 1.667$) the same $Br_{H2}$ results in a 1.5% decrease in $Nu_{H2}$ for heating, and a 1.5% increase in $Nu_{H2}$ for cooling. This reduced effect of $Br_{H2}$ on $Nu_{H2}$ with increasing $\beta_{v1}Kn$ is due to the reduced velocity gradients caused by increasing slip at the wall. Although trends in $Nu_{H2}$ due to viscous dissipation and rarefaction are the same for all $AR$ investigated, these effects are more significant for $AR = \infty$ than for $AR = 1$, 2, and 5. This is because the parallel plate channel has larger velocity gradients, resulting in increased viscous dissipation, and with no side wall heat flux contribution, the thermal energy generated by viscous dissipation is relatively more significant.

The $Nu_T$ data presented in Fig. 4 with viscous dissipation effects, $Br_T \neq 0$ were obtained for $Pe = 0.5$ and $Br_T = -0.2$;

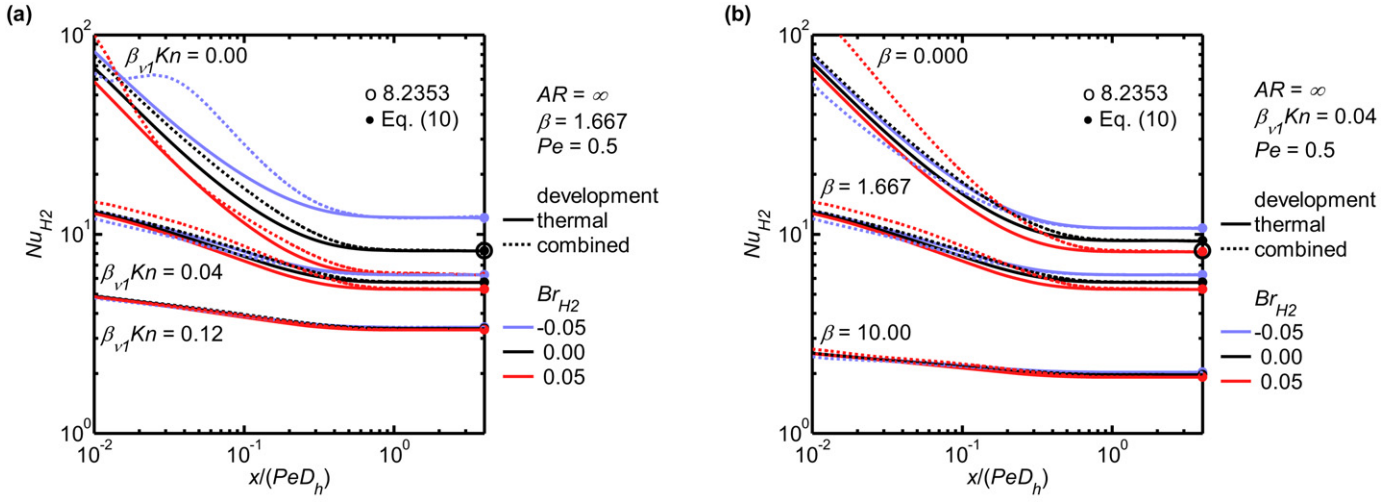


Fig. 5. Thermally and hydrodynamically developing $Nu_{H2}$: (a) effect of $\beta_{v1}Kn$ and $Br_{H2}$, (b) effect of $\beta$ and $Br_{H2}$.

however, for a given $\beta_{v1}Kn$, $\beta$, $AR$, and slip boundary condition model, all flows with viscous dissipation and flow work result in the same fully developed value of $Nu_T$, regardless of the magnitude of $Pe$ or $Br_T$. As discussed previously, for continuum flow, the thermal energy generated by viscous dissipation, predominantly near the walls due to the larger velocity gradients, is equal to the thermal energy absorbed by flow work, predominantly near the center of the flow due to the larger velocity magnitudes. This energy balance results in $\partial T_m/\partial x = 0$, a net wall heat flux of zero, and therefore $Nu_T = 0$ for the constant wall temperature boundary condition. Within the slip flow regime, the slip flow at the wall reduces both the average cross sectional velocity gradients and the maximum core velocity. Although this results in a decrease in both the thermal energy generated by viscous dissipation, and the thermal energy absorbed by flow work, the decrease in viscous dissipation is more significant. The difference, however, is exactly equal to the thermal energy generated by shear work at the wall due to the slipping flow – meaning that, viscous dissipation, flow work, and shear work are still balanced energy sources and sinks, i.e. $\partial T_m/\partial x = 0$, regardless of the magnitude of $Br_T$ or $Pe$ [6]. However, the shear work at the wall creates a nonzero wall heat flux and therefore a nonzero $Nu_T$. The shear work, $u\partial\tau/\partial y|_{y=0}$, is a function of both the slip velocity and the wall normal velocity gradients. As $\beta_{v1}Kn$ increases, the slip velocity increases, and for the lower slip flow regime this increases the shear work and therefore increases $Nu_T$. However, as the slip velocity increases the velocity gradients throughout the flow decrease, and for the upper end of the slip regime this leads to a decrease in the shear work (for $AR = \infty$, the point of maximum shear work is $\beta_{v1}Kn = 0.083$). These effects, combined with the effect of $AR$ and temperature jump ($\beta \neq 0$), which, decreases the energy exchange with increasing $\beta_{v1}Kn$, result in the $Nu_T$ trends displayed in Fig. 4.

### 4.2. Thermally and hydrodynamically developing Nu

Numerical results for thermally and hydrodynamically developing parallel plate $Nu_{H2}$ and $Nu_T$ are presented in Figs. 5 and 6 as functions of $x/PeD_h$ (the nondimensional axial distance), $\beta_{v1}Kn, \beta, Br$, and $Pe$. For these data, first-order slip boundary conditions, without creep flow, are used. Thermally developing flow is represented by the solid lines, and thermally/hydrodynamically developing flow, 'combined' flow, is represented by the dotted lines. To verify the accuracy of the numerical data, and that the flow has reached a locally fully developed state, analytic solutions for fully developed $Nu$, Eq. (10) for $Nu_{H2}$, and Eq. (12) for $Nu_T$, are displayed as solid symbols at $x/PeD_h = 4$, the channel outlet. Also, conventional fully developed parallel plate $Nu$, without rarefaction or viscous dissipation effects, $Nu_{H2} = 8.2353$ in Fig. 5 and $Nu_T = 8.0582$ ($Pe = 0.5$) in Fig. 6, are displayed as circles at $x/Pe\,D_h = 4$ to serve as a point of reference for changes in $Nu$ due to rarefaction, viscous dissipation, and developing flow effects. Additionally, to demonstrate the basis of the thermally/hydrodynamically developing $Nu_{H2}$ and $Nu_T$ results presented in Figs. 5 and 6, velocity profiles and temperature profiles (relative to $T_w$) for several cases are illustrated in Fig. 7.

Thermally and hydrodynamically developing $Nu_{H2}$, with viscous dissipation effects, are given in Fig. 5 for various levels of $\beta_{v1}Kn$, Fig. 5(a), and $\beta$, Fig. 5(b). Temperature profiles for thermally/hydrodynamically developing flow, with constant wall heat flux thermal boundary conditions, $\beta = 1.667$, $Pe = 0.5$, $\beta_{v1}Kn = 0.00$ and 0.04, and $Br_{H2} = \pm 0.05$ are illustrated in Fig. 7(b). Again, negative $Br_{H2}$ indicates cooling, positive $Br_{H2}$ denotes heating and $Br_{H2} = 0$ signifies no viscous dissipation effect. For the flows examined in Fig. 5, the average $Nu_{H2}$ entrance length (i.e., distance from the channel entrance where $Nu(x) = 0.99Nu_\infty$) is roughly $1.0Pe\,D_h$, and varies little for each of the parameters varied – entrance length increases slightly for combined developing flow, lower values of $\beta_{v1}Kn$, lower values of $\beta$, and negative $Br_{H2}$. As may be expected based on the fully developed $Nu_{H2}$ results presented previously, these results indicate that increasing $\beta_{v1}Kn$, Fig. 5(a), or increasing $\beta$, Fig. 5(b), result in a decrease in $Nu_{H2}$ for both developing and fully developed flow. The effect of $Br_{H2}$ on hydrodynamically fully developed flow, shown previously in

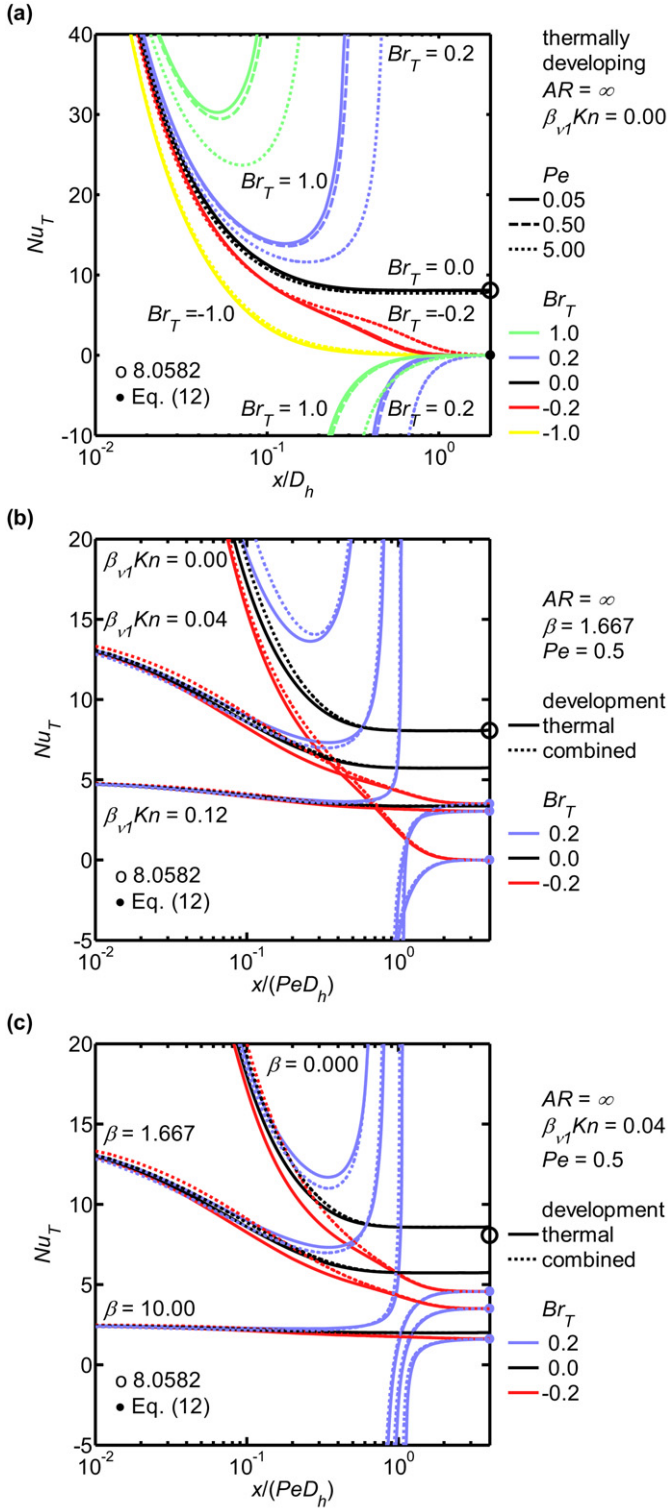


Fig. 6. Thermally and hydrodynamically developing $Nu_T$: (a) effect of $Pe$ and $Br_T$, (b) effect of $\beta_{v1}Kn$ and $Br_T$, (c) effect of $\beta$ and $Br_T$.

Figs. 3(a) and 4, is to increase the wall temperature, which, for heating, increases the wall-mean temperature difference and decreases $Nu_{H2}$, and for cooling, decreases the wall-mean temperature difference and increases $Nu_{H2}$. This $Br_{H2}$ effect is also evident in the developing $Nu_{H2}$ presented in Figs. 5 and 7(b). Developing $Nu_{H2}$ are larger at the channel inlet, compared to fully developed values, due to the initially small wall-mean temperature difference $|T_w - T_m|$, as illustrated in Fig. 7(b).

Thermally/hydrodynamically developing flows also have large velocities near the wall at the channel inlet, which tends to increase $Nu_{H2}$ beyond that of thermally developing flow alone, as evident in Fig. 5 for $Br_{H2} = 0$. Thermally/hydrodynamically developing flows with $Br_T \neq 0$, additionally, have viscous dissipation and flow work effects that are a function of the hydrodynamic flow development, which, as may be surmised from the velocity profiles in Fig. 7(a), are initially concentrated immediately next to the channel wall at the inlet. For continuum flow, $\beta_{v1}Kn = 0$, at $0.01\,Pe\,D_h$, the dominant effect, moving from the wall to the center of the flow, is first viscous dissipation, then flow work, followed by viscous dissipation again. At $0.01\,Pe\,D_h$ heat conducted at the wall does not yet have a significant effect through the center of the flow, and changes in the temperature profile are primarily due to viscous dissipation and pressure flow effects. As a result of the counteracting viscous dissipation and flow work effects closest to the wall, $T_w$ is slightly decreased, compared to thermally developing flow, and due to the viscous dissipation effect nearest to the center of the flow, the temperature at the center of the flow is slightly increased, compared to thermally developing flow. Because $|T_w - T_m|$ is initially very small, this results in an increase in $Nu_{H2}$ for heating, and decrease in $Nu_{H2}$ for cooling, compared to thermally developing flow, as displayed in Fig. 5(a), for $\beta_{v1}Kn = 0$ and $0.01\,Pe\,D_h$. As the velocity profile develops, the large viscous dissipation and flow work effects near the wall are distributed through the channel and the second region of viscous dissipation is eliminated. As this occurs, viscous dissipation and flow work create a temperature gradient that is conducive to heating, but has an insulating effect for cooling. This results in an accelerated temperature profile development for heating, and a slowed temperature profile development for cooling, as displayed in Figs. 5(a) and 7(b) for $\beta_{v1}Kn = 0$, $Br_{H2} = \pm 0.05$, and $\sim 0.032$–$0.32\,Pe\,D_h$. In a rarified flow, $\beta_{v1}Kn \neq 0$, slip flow significantly reduces the velocity and pressure gradients at the channel inlet. Compared to continuum flow, this both reduces the magnitude, and alters the distribution of the viscous dissipation and flow work effects. With increased slip near the inlet, flow work is the most significant effect immediately next to the wall (for the $\beta_{v1}Kn$ values examined here). This results in a decrease in $|T_w - T_m|$ for heating, an increase in $|T_w - T_m|$ for cooling, and consequently an increase in $Nu_{H2}$ for $+Br_{H2}$, and a decrease in $Nu_{H2}$ for $-Br_{H2}$, compared to flows that are only developing thermally, as displayed in Fig. 5, for $\beta_{v1}Kn \neq 0$ and $\pm Br_{H2}$. As the flow develops hydrodynamically, viscous dissipation and flow work effects are distributed throughout the cross section of the flow, with viscous dissipation acting predominantly at the walls and flow work acting predominantly at the center of the flow, and the fully developing $Nu_{H2}$ values discussed previously are achieved.

Thermally and hydrodynamically developing $Nu_T$, with viscous dissipation effects, are given in Fig. 6 for various levels of $Pe$, Fig. 6(a), $\beta_{v1}Kn$, Fig. 6(b), and $\beta$, Fig. 6(c). Temperature profiles for thermally/hydrodynamically developing flow, with

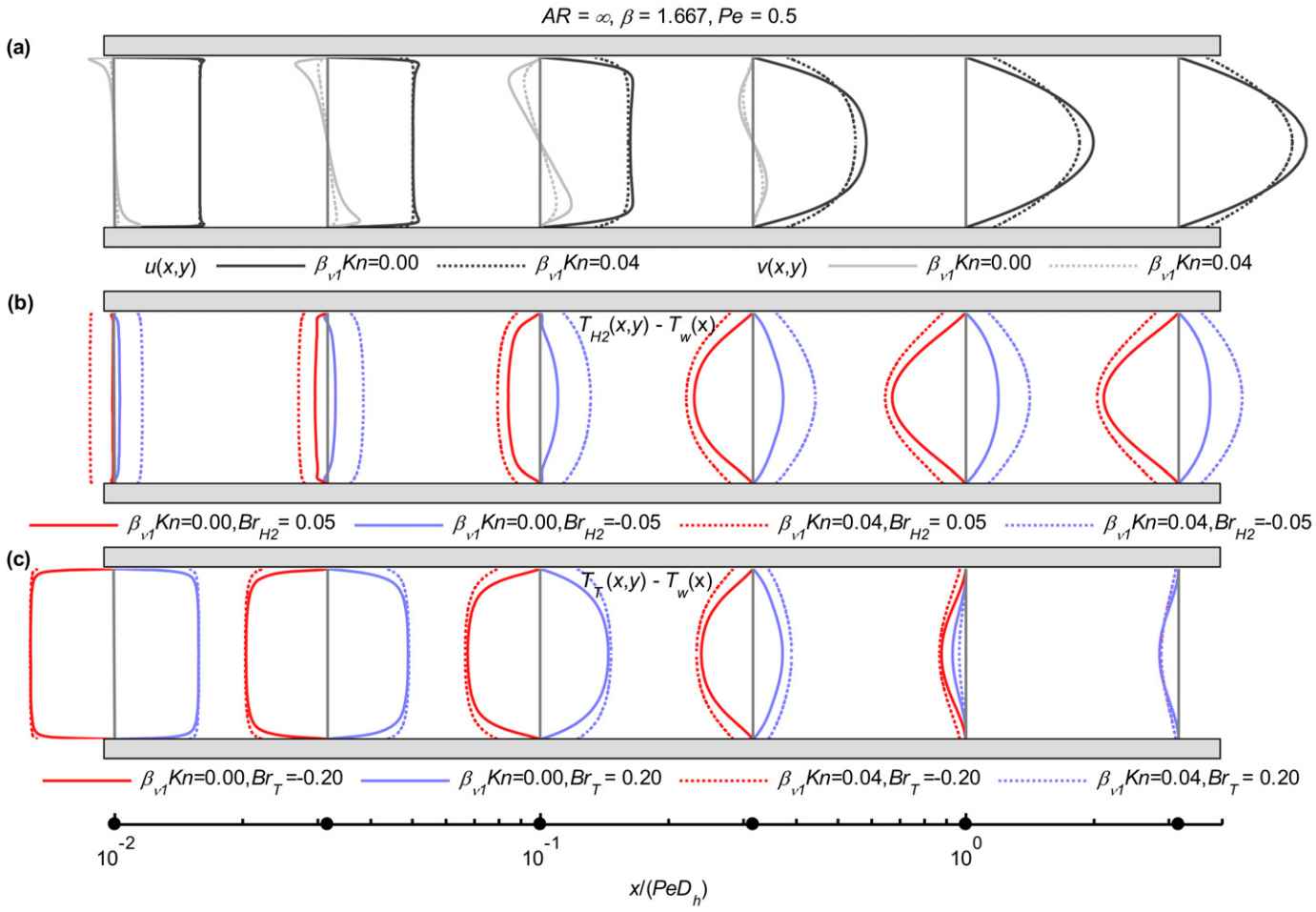


Fig. 7. Thermally/hydrodynamically developing flow: (a) $u(x, y)$ and $v(x, y)$, (b) $T_{H2}(x, y)$, (c) $T_T(x, y)$.

constant wall temperature boundary conditions, $\beta = 1.667$, $Pe = 0.5$, $\beta_{v1}Kn = 0.00$ and 0.04, and $Br_T = \pm 0.20$ are illustrated in Fig. 7(c). Negative $Br_T$ indicates heating, positive $Br_T$ denotes cooling, and $Br_T = 0$ signifies no viscous dissipation effect. For the flows examined in Fig. 6, $Nu_T$ entrance lengths are between approximately $0.5\,Pe\,D_h$ and $4\,Pe\,D_h$, where the entrance length increases for $Br_T \neq 0$ (most significantly for positive $Br_T$), higher values of $Pe$, lower values of $\beta_{v1}Kn$, lower values of $\beta$, and thermally/hydrodynamically developing flow. The data in Fig. 6(a) demonstrate the effect of $Pe$ and $Br_T$ on thermally developing $Nu_T$, for continuum flow, $\beta_{v1}Kn = 0$. For cases when viscous dissipation is negligible, $Br_T = 0$, the developing mean fluid temperature approaches the wall temperature, for either heating or cooling, and fully developed $Nu_T$ is a function of $Pe$. When viscous dissipation and flow work effects are considered ($Br_T \neq 0$), the developing mean fluid temperature, for either heating or cooling, approaches a constant that is less than the wall temperature by an amount dependent on the magnitude of $Br_T$. The resulting fully developed $Nu_T$, as predicted by Eq. (12), and discussed previously, is not a function of the magnitude of $Br_T$ or $Pe$. These developing $Nu_T$ results are most comprehendible when viewed in conjunction with the temperature profiles illustrated in Fig. 7(c) for $\beta_{v1}Kn = 0$ (although, these are for hydrodynamically developing flow). Developing $Nu_T$ are larger at the channel entrance, due to the large temperature gradients at the wall. As the temperature profile develops, $Nu_T$ initially decreases for both heating and cooling. $Nu_T$ for cooling however, reaches a minimum at the axial location were the heat conduction from the wall reaches the center of the flow [12]. As the mean fluid temperature of the cooling flow continues to decrease, due to the effect of flow work, $Nu_T$ exhibits a singularity point where $T_m = T_w$, and is negative just after this when $T_m < T_w$ ($q_w$ is still negative). For continuum non-slip flow, $q_w$ for both heating and cooling, approaches zero, resulting in a fully developed $Nu_T$ value of zero. For slip flow, the fully developed $q_w$ is positive, not zero, due to the effect of shear work at the wall. This results in a positive, nonzero fully developed $Nu_T$, which for a given value of $\beta_{v1}Kn$ and $\beta$, is the same for either heating or cooling, and does not depend on the magnitude of $Br_T$, as has been discussed previously with the fully developed $Nu_T$ results presented in Fig. 4. Many of the effects of hydrodynamically developing flow on $Nu_T$, displayed in Figs. 6(a) and 6(b), are similar to those discussed previously for hydrodynamically developing $Nu_{H2}$. For $Br_T = 0$, hydrodynamically developing flow initially increases $Nu_T$, compared to thermally developing $Nu_T$. For $Br_T \neq 0$ and $\beta_{v1}Kn = 0$, $Nu_T$ initially increases, followed by an accelerated thermal development for heating, and for cooling $Nu_T$ initially decreases fol-

lowed by a slowed thermal development (this effect however, is much less significant for $Nu_T$, than for $Nu_{H2}$, and consequently is not displayed in Fig. 6). For $Br_T \neq 0$ and $\beta_{v1}Kn \neq 0$, hydrodynamically developing slip flow results in flow work adjacent to the wall that initially increases $Nu_T$ for heating and decreases $Nu_T$ for cooling, compared to thermally developing $Nu_T$.

## 5. Summary and conclusions

The effect of viscous dissipation and rarefaction on rectangular microchannel convective heat transfer is numerically evaluated subject to constant wall heat flux ($H2$) and constant wall temperature ($T$) thermal boundary conditions in the slip flow regime. $Nu_{H2}$ and $Nu_T$ are presented in terms of the degree of rarefaction ($\beta_{v1}Kn$); the gas–wall interaction parameter ($\beta$); viscous dissipation ($Br_{H2}$ or $Br_T$); and axial conduction ($Pe$). These results are valid for nearly incompressible, steady state flows. Numerical results are obtained using a continuum based, three-dimensional, compressible, unsteady CFD algorithm, modified with slip velocity and temperature jump boundary conditions. To verify the numerical results, analytic solution for thermally and hydrodynamically fully develop $Nu_{H2}$ and $Nu_T$ are derived for the limiting case of parallel plate channels.

Both analytical and numerical data indicate that effects of viscous dissipation, flow work, and axial conduction are all significant within the slip flow regime for thermally/hydrodynamically developing and locally fully developed Nusselt numbers. The significance of each of these terms depends on the degree of rarefaction, the gas–wall interactions, and the heating configuration. Viscous dissipation effects may either increase or decrease $Nu$ depending on the heating configuration, and are reduced with increasing rarefaction. Viscous dissipation increases $Nu_{H2}$ for cooling, and decreases $Nu_{H2}$ for heating as a function of $Br_{H2}$, $\beta_{v1}Kn$, $\beta$, and $AR$. The combined effects of viscous dissipation, flow work, and shear work within the slip flow regime cause $Nu_T$ to increase, from zero for continuum flow, with increasing $\beta_{v1}Kn$ by an amount dependent on $AR$ and $\beta$ but not on the magnitude of $Br_T$ or $Pe$. Based on the results presented for rarified, constant wall temperature flows, the effects of flow work and shear work may not be assumed to be negligible when viscous dissipation is a significant parameter.

## Acknowledgements

Partial support of this work by National Science Foundation grant number DGE9987616, of the Integrative Graduate Education and Research Traineeship Program, and US Department of Energy grant number W-7405-ENG-48, through the Center for the Simulation of Accidental Fires and Explosions, is gratefully acknowledged.

## References

[1] J.C. Maxwell, On stresses in rarified gases arising from inequalities of temperature, Philosophical Transactions of the Royal Society of London 170 (1879) 231–256.
[2] M. Smoluchowski, Ueber Wärmeleitung in Verdünnten Gasen, Annalen der Physik und Chemie 64 (1898) 101–130.
[3] G.E. Karniadakis, A. Beskok, Micro Flows: Fundamentals and Simulation, Springer-Verlag, New York, 2002.
[4] J. Maurer, P. Tabeling, P. Joseph, H. Willaime, Second-order slip laws in microchannels for helium and nitrogen, Physics of Fluids 15 (2003) 2613–2621.
[5] S. Colin, P. Lalonde, R. Caen, Validation of a second-order slip flow model in rectangular microchannels, Heat Transfer Engineering 25 (2004) 23–30.
[6] N.G. Hadjiconstantinou, Dissipation in small scale gaseous flows, Journal of Heat Transfer 125 (2003) 944–947.
[7] T.N. Aynur, L. Kuddusi, N. Egrican, Viscous dissipation effect on heat transfer characteristics of rectangular microchannels under slip flow regime and H1 boundary conditions, Heat and Mass Transfer 42 (2006) 1093–1101.
[8] C.-H. Chen, Slip-flow heat transfer in a microchannel with viscous dissipation, Heat and Mass Transfer 42 (2006) 853–860.
[9] H.-E. Jeong, J.-T. Jeong, Extended Graetz problem including streamwise conduction and viscous dissipation in microchannel, International Journal of Heat and Mass Transfer 49 (2006) 2151–2157.
[10] O. Aydin, M. Avci, Analysis of laminar heat transfer in micro-Poiseuille flow, International Journal of Thermal Sciences 46 (2007) 30–37.
[11] K. Hooman, Entropy generation for microscale forced convection: Effects of different thermal boundary conditions, velocity slip, temperature jump, viscous dissipation, and duct geometry, International Communications in Heat and Mass Transfer 34 (2007) 945–957.
[12] J.W. Ou, K.C. Cheng, Effects of flow work and viscous dissipation on Graetz problem for gas flows in parallel-plate channels, Heat and Mass Transfer 6 (1973) 191–198.
[13] R.K. Shah, A.L. London, Laminar Flow Forced Convection in Ducts, Academic Press, New York, 1978.
[14] M. Renksizbulut, H. Niazmand, G. Tercan, Slip-flow and heat transfer in rectangular microchannels with constant wall temperature, International Journal of Thermal Sciences 45 (2006) 870–881.
[15] H.P. Kavehpour, M. Faghri, Y. Asako, Effects of compressibility and rarefaction on gaseous flows in microchannels, Numerical Heat Transfer, Part A: Applications 32 (1997) 677–696.
[16] C. Hong, Y. Asako, S.E. Turner, M. Faghri, Friction factor correlations for gas flow in slip flow regime, Journal of Fluids Engineering 129 (2007) 1268–1276.
[17] R.M. Inman, Laminar slip flow heat transfer in a parallel-plate channel or a round tube with uniform wall heating, NASA TN D-2393, 1964.
[18] J. van Rij, T. Harman, T. Ameel, The effect of creep flow on two-dimensional isoflux microchannels, International Journal of Thermal Sciences 46 (2007) 1095–1103.
[19] J. van Rij, T. Ameel, T. Harman, The effect of viscous dissipation on two-dimensional microchannel heat transfer, in: Proceedings of 2006 ASME International Mechanical Engineering Congress and Exposition IMECE2006, Chicago, IL, United States, 2006.
[20] J. van Rij, T. Ameel, T. Harman, Constant wall temperature Nusselt and Poiseuille numbers in rectangular microchannels, in: Proceedings of 2007 ASME–JSME Thermal Engineering Summer Heat Transfer Conference HT2007, Vancouver, BC, Canada, 2007.
[21] J. van Rij, T. Ameel, T. Harman, Effects of creep flow and viscous dissipation in the slip regime for isoflux rectangular microchannels, in: Proceedings of 2007 ASME International Mechanical Engineering Congress and Exposition IMECE2007, Seattle, WA, United States, 2007.
[22] B.A. Kashiwa, N.T. Padial, R.M. Rauenzahn, W.B. VanderHeyden, A cell-centered ICE method for multiphase flow simulations, Los Alamos National Laboratory Technical Report LA-UR-93-3922, 1993.
[23] S.G. Parker, J. Guilkey, T. Harman, A component-based parallel infrastructure for the simulation of fluid–structure interaction, Engineering with Computers 22 (2006) 277–292.
[24] J.E. Guilkey, T.B. Harman, B. Banerjee, An Eulerian–Lagrangian approach for simulating explosions of energetic devices, Computers and Structures 85 (2007) 660–674.
[25] S. Yu, Slip flow heat transfer in rectangular microchannels, Ph.D. thesis, University of Utah, USA, 2002.